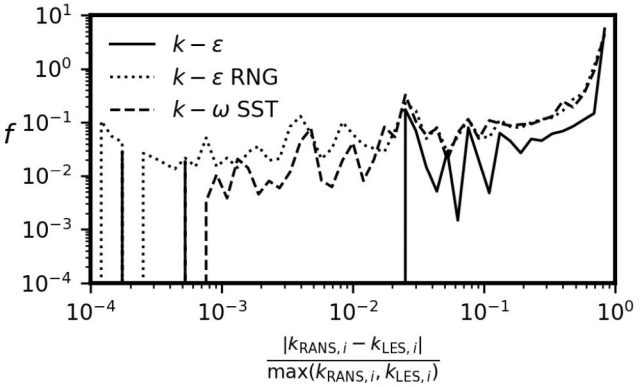

Figure 4. Error distribution function comparing LES with RANS simulations. Standard $k-\varepsilon$ (solid line); $k-\varepsilon$ RNG (dotted line); and $k-\omega$ SST (dashed line).

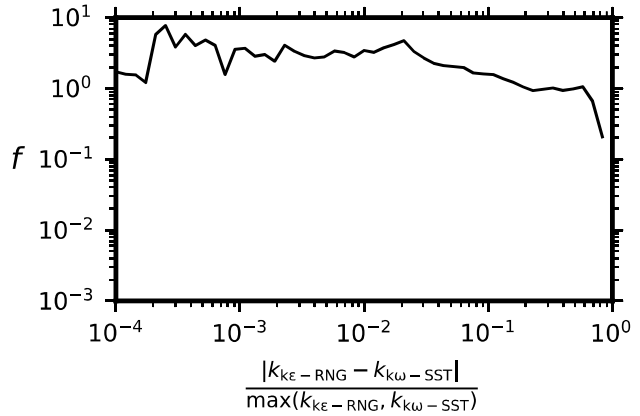

Figure 5. Error distribution function comparing the $k-\varepsilon$ RNG and $k-\omega$ SST models.

3. Population Balance Model

In this section, the employed PBM is detailed. As mentioned in Section 2, the interplay between fluid dynamics and precipitation determines the final primary particles. In this contribution, the coupling between the fluid dynamics and the precipitation phenomena was obtained through implementing the β-Probability Density Function (PDF) approach. In this approach, two equations are used to model the multi-scale nature of precipitation. One equation is employed to track the evolution of the mixture fraction, $\bar{\alpha}$, and the other is used to track the evolution of the variance in the mixture fraction, $\bar{\alpha}'^2$. The mixture fraction describes the macro-mixing, whereas its variance describes the micro-mixing. In the RANS framework, the transport equation for $\bar{\alpha}$ is as follows:

$$\frac{\partial \bar{\alpha}}{\partial t} + \bar{\mathbf{u}}\nabla\bar{\alpha} = D_t\nabla^2\bar{\alpha} \tag{10}$$

and the transport equation for its variance is as follows:

$$\frac{\partial \bar{\alpha}'^2}{\partial t} + \bar{\mathbf{u}}\cdot\nabla\bar{\alpha}'^2 = D_t\nabla^2\bar{\alpha}'^2 + 2D_t(\nabla\bar{\alpha}\cdot\nabla\bar{\alpha}) - \epsilon_{\bar{\alpha}'^2} \tag{11}$$

In addition to the accumulation, advection, and diffusion, Equation (11) has two other terms to analyze. The production term, $2D_t(\nabla\bar{\alpha}\cdot\nabla\bar{\alpha})$, is related to the macro-scale, where variance is generated, and the dissipation term $\epsilon_{\bar{\alpha}'^2}$, is related to the smallest scale (i.e., the

Batchelor scale), where it is dissipated. Unlike the production, the dissipation term requires a closure equation [13]:

$$\epsilon_{\bar{\alpha}'^2} = \gamma \overline{\alpha'^2} \tag{12}$$

$$\gamma = \frac{C_\phi}{2} \frac{\varepsilon}{k} \tag{13}$$

According to our previous publications [22,24], C_ϕ was set to be equal to 2. This approach, therefore, can account for the dumping effect of mixing on the chemical reaction. In other words, Mg^{2+} and OH^- have to macro- and micro-mix before they can react according to Equation (1), hindering the precipitation process. In our previous publication [22] (Supplementary Materials), we derived an analytical solution through coupling the reactant concentration htat was fed into the system with the amount that is physically able to react (i.e., the amount of reactants at the micro-scale) after mixing to form the $Mg(OH)_2$. For the sake of clarity, only the final equation is reported:

$$[Mg(OH)_2]_{(aq)} = \min\left(\left[Mg^{2+}\right], \frac{[OH^-]}{2}\right) f\left(\bar{\alpha}, \bar{\alpha}'^2, \bar{\alpha_s}\right) \tag{14}$$

where Mg^{2+} and OH^- are the concentration values in the system and $f\left(\bar{\alpha}, \bar{\alpha}'^2, \bar{\alpha_s}\right)$ is the weighting function accounting for mixing. $\bar{\alpha}_s$ is the stoichiometric mixture fraction, defined as follows:

$$\bar{\alpha}_s = \frac{2\left[Mg^{2+}\right]^{(in)}}{2[Mg^{2+}]^{(in)} + [OH^-]^{(in)}} \tag{15}$$

where apex "(in)" represents the reactant concentration at the inlets. This represents, in the mixture fraction space, the mixture fraction value at which the reactants can stoichiometrically react. Assuming that the $Mg(OH)_{2(aq)}$ in the aqueous phase instantaneously precipitates in its solid form, we can define the supersaturation as follows:

$$S = \frac{\gamma_\pm^3 [Mg^{2+}]_{(aq)} [OH^-]^2_{(aq)}}{k_{sp}} - 1 \tag{16}$$

where $[Mg^{2+}]_{(aq)}$ and $[OH^-]_{(aq)}$ are calculated for stoichiometry using Equation (14), $\gamma_\pm$ is the activity coefficient, and k_{sp} is the solubility product, which is equal to $10^{-10.88}$. Supersaturation build-up, therefore, triggers precipitation processes. In this contribution, we accounted for primary nucleation (both homogeneous and heterogeneous), J:

$$J = \underbrace{A_1 e^{\left(-\frac{B_1}{\ln^2(S+1)}\right)}}_{\text{Homogeneous}} + \underbrace{A_2 e^{\left(-\frac{B_2}{\ln^2(S+1)}\right)}}_{\text{Heterogeneous}} \tag{17}$$

and molecular growth, G:

$$G = k_g S^g \tag{18}$$

Equations (17) and (18) have six tuning parameters (A_1, B_1, A_2, B_2, k_g, and g). A_i and B_i model the intensity of primary nucleation, k_g represents the intensity of the molecular growth, and g is related to the growth mechanism (g = 1 corresponds to a diffusion-controlled mechanism). The aggregation rate, β_{agg}, is as follows:

$$\beta_{agg} = \beta_{col} \eta_{agg} \tag{19}$$

The aggregation rate is proportional to the collision frequency, β_{col}, representing the number of collisions per unit time between primary particles, and to the sticking probability, η_{agg},

which represents the probability that these events are effective (i.e., whether the primary particle will cement or not). The collision frequency accounts for both the Brownian and turbulent contributions.

$$\beta_{col} = 10^{C_1}(\beta_{br} + \beta_{tr}) \tag{20}$$

The Brownian contribution is described by the following equation:

$$\beta_{br} = \frac{2k_B T}{3\mu}\frac{(L+\lambda)^2}{L\lambda} \tag{21}$$

where k_B is the Boltzmann constant, T is the fluid temperature, μ is the fluid dynamic viscosity, and L and λ are the sizes of the colliding particles. The turbulent contribution, instead, has the following form:

$$\beta_{tr} = \sqrt{\frac{8\pi}{15}}\sqrt{\frac{\varepsilon}{\nu}}\frac{(L+\lambda)^3}{2} \tag{22}$$

The sticking probability equation, on the other hand, can be modelled as follows:

$$\eta_{agg} = e^{-\theta} \tag{23}$$

where θ denotes the ratio of the cementation time, t_{cem}, and the interaction time, t_{int}. The interaction time is defined as the characteristic time of the Kolmogorov micro-scale:

$$t_{int} = \sqrt{\frac{\nu}{\varepsilon}} \tag{24}$$

and represents the duration during which the two particles remain in close proximity and interact, while the cementation time is defined as follows:

$$t_{cem} = \frac{D_b}{s(\delta)G} \tag{25}$$

$$D_b = \frac{L_{eqv}\rho_p^{0.5}(\varepsilon\nu)^{0.25}}{A_p^{0.5}} \tag{26}$$

$$L_{eqv} = \frac{L\lambda}{(L^2+\lambda^2-L\lambda)^{0.5}} \tag{27}$$

This represents the time needed for the irreversible cementation of two primary particles. $s(\delta)$ is a shape function, defined as follows [29]:

$$s(\delta) = \frac{4\left(1+\delta-\delta'\right)}{1/3+\delta-\delta'-\left(\delta-\delta'\right)^2\left(2\delta/3+\delta'/3\right)} \tag{28}$$

$$\delta = L/\lambda \tag{29}$$

$$\delta' = \sqrt{\delta^2-1} \tag{30}$$

Equations (20) and (26) have two additional tuning parameters (C_1 and A_p). C_1 modules the collision frequency intensity and A_p is proportional to the crystalline bridge strength between primary particles. In our previous publications, we provided innovative machine learning-based methodologies to identify their values [23], fitted our model [22], and validated it [24]. Therefore, only their values are reported here (Table 2).

Table 2. Kinetics parameters set from Raponi and Marchisio [23].

	A_1	A_2	B_1	B_2	k_g	g	C_1	A_p
Parameter value	$10^{25.45}$	$10^{15.4}$	301	57	$10^{-11.15}$	1.5	0.79	5.3
Units	$\frac{\text{particle no.}}{\text{m}^3\text{s}^1}$		-	-	$\frac{\text{m}}{\text{s}}$	-	-	$\frac{\text{N}}{\text{m}^2}$

The evolution of the primary particles due to the precipitation phenomena described above was tracked through applying the Quadrature Method of Moments (QMOM) [14,30]. The transport equation for the k-th moment is as follows:

$$\frac{\partial \bar{m}_k}{\partial t} + \bar{\mathbf{u}} \cdot \nabla \bar{m}_k = D_t \nabla^2 \bar{m}_k + \dot{h}_k \quad (31)$$

$$\dot{h}_k = J L_c^k + k G m_{k-1} + \overline{B}_k - \overline{D}_k \quad (32)$$

where L_c is the critical size (1 nm) for a stable nucleus and $\overline{B}_k$ and $\overline{D}_k$ model the birth and death contributions due to aggregation. In this contribution, we used three quadrature nodes, leading to six moments. To conclude, the PBM was closed using the mass balances for the reacting species ($[Mg^{2+}]$ and $[OH^-]$):

$$\frac{\partial \bar{c}_i}{\partial t} + \bar{\mathbf{u}} \cdot \nabla \bar{c}_i = D_t \nabla^2 \bar{c}_i - \frac{\nu_i \rho_p k_v}{M_p} \dot{h}_3 \quad (33)$$

where ν_i is the stoichiometric coefficient (i.e., $\nu_{Mg^{2+}} = 1$ and $\nu_{OH^-} = 2$), ρ_p corresponds to the particle density, M_p is the molecular weight, $k_v = \pi/6$ is the shape factor, and $\dot{h}_3$ is the third-order moment sink term. We used a one-way approach for the CFD-PBM. The flow and turbulence fields extracted from the steady-state RANS solution and passed to the PBM were used as constant inputs. These quantities were used to compute the mixing and aggregation for use in the population balance model. Given the low solids concentration and the sub-micron/micron size of the $Mg(OH)_2$ particles, the particle–fluid interactions are negligible, justifying the one-way coupling approach [22].

4. Results

We report two investigations: (i) the influence of the reactant concentration at constant flow and turbulence fields and (ii) the influence of the nozzles orientation at constant reactant concentrations.

(i) Effect of the reactant concentration

To assess the influence of the reactant concentration, three values for Mg^{2+} concentration (0.1, 0.3, and 0.6 M) and three for OH^- (0.005, 0.01, and 0.02 M) were selected, resulting in a matrix of nine elements. These concentration values were selected to reflect the operational ranges in the pilot plant, based on the inlet flow rates and chemical compositions that are typically handled. The analysis was performed with the same flow and turbulence fields. In this regard, the same geometry only had two nozzles: one pointing in a high-velocity region and another pointing in a low-velocity region. This decision was made so as not to lose generality. Since the geometry is constant, this implies that the mixture fraction and its variance remain constant across all operating conditions. Equations (10) and (11) are functions of the turbulence fields only. Figure 6 shows both the mixture fraction and its variance in the streamlines that the particles would follow if they started from the two nozzles (the model assumes a one-way coupling approach).

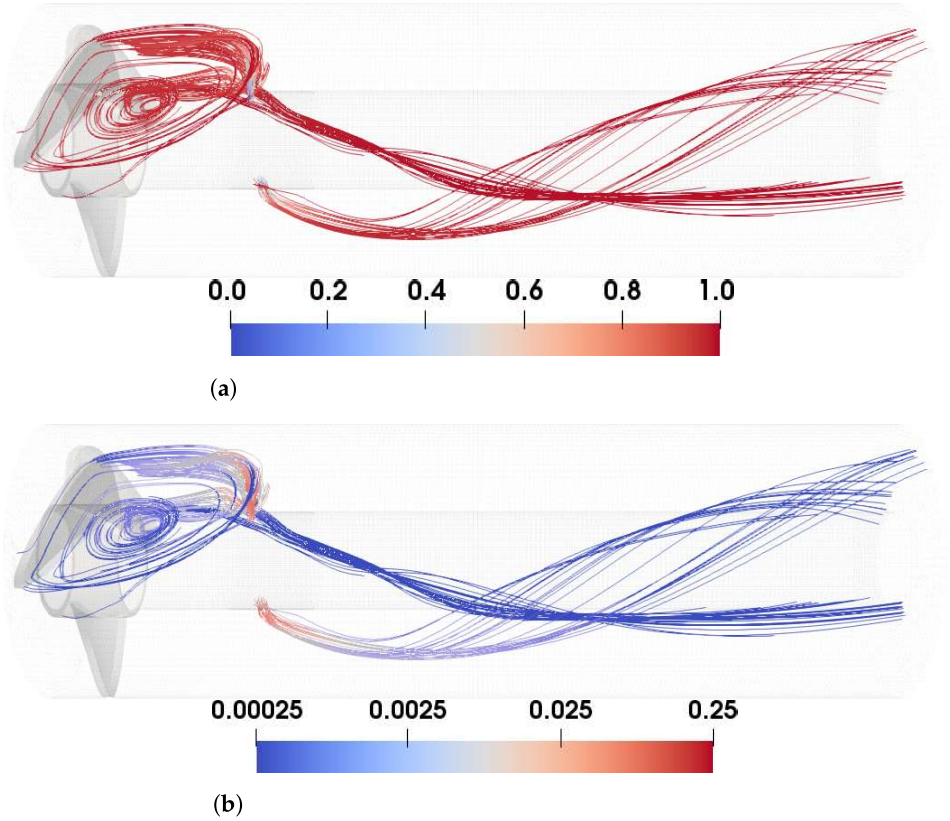

Figure 6. Visualization of the mixture fraction (**a**) and its variance (**b**) for the two nozzles' configuration.

Figure 6 shows that complete mixing occurs soon after the two nozzles. The Mg^{2+} jet entering the circular crown locally alters the mixing fraction (depicted in light blue in Figure 6a). As a result, macro-scale mixing leads to micro-scale segregation, as shown by the red regions around the nozzles in Figure 6b. This investigation, therefore, aims to show how strongly mixing can hinder precipitation processes as a function of the reactant concentration, especially when the ultimate goal is the reactor manufacturing. It is important to emphasize that, even though the flow field, mixture fraction, and its variance remain unchanged across all operating conditions, this does not imply that the mixing conditions are identical. In fact, the mixing weight function in Equation (14) is a function of the stoichiometric mixture fraction, which is a function of the reactant concentration entering the system. As a result, increasing the concentration consistently raises the first term in Equation (14) ($\min([Mg^{2+}], 2[OH^-])$). However, the effect on the second term (f) is not straightforward, as it depends on the local value of $\bar{\alpha}$ relative to $\bar{\alpha_s}$. The corresponding $\bar{\alpha_s}$ values for all nine simulations are listed in Table 3.

Table 3. $\bar{\alpha}_s$ values used in the simulations.

$[Mg^{2+}]^{(in)}$, M	$[OH^-]^{(in)}$, M		
	0.005	**0.01**	**0.02**
0.1	0.976	0.952	0.909
0.3	0.992	0.984	0.968
0.6	0.996	0.992	0.984

The two variables used for comparison are both the supersaturation, S, and the zeroth order moment, m_0. Figure 7 presents the results for the supersaturation.